Pakistan Veterinary Journal

ISSN: 0253-8318 (PRINT), 2074-7764 (ONLINE)
DOI: 10.29261/pakvetj/2026.190

RESEARCH ARTICLE

Gambogenic Acid Inhibits Tumor Angiogenesis and Growth in Canine Osteosarcoma via Fibronectin Type III and SPRY Domain Containing 1 (FSD 1) Modulation

Meimei Wang‡, Guangmin Zhang‡, Junping Sun‡, Huijie Kang, Siyao Li, Weiqian Wang, Qingdian Hou, Pujun Li, Xinru Li, Bingsong Yang, Honggang Fan* and Yuan Zhao*

Heilongjiang Provincial Key Laboratory of Pathogenic Mechanism for Animal Disease and Comparative Medicine, Northeast Agricultural University, Harbin, 150030, China. ‡Meimei Wang, Guangmin Zhang, and Junping Sun contributed equally to this work.
*Corresponding author: fanhonggang2002@163.com; 16645266261@163.com

ARTICLE HISTORY (26-590)

Received: May 15, 2026
Revised: July 03, 2026
Accepted: July 12, 2026
Published online: August 16, 2026

Key words:
Canine osteosarcoma
Fibronectin type III and SPRY domain containing 1 (FSD1)
Gambogenic acid
Tumor angiogenesis

ABSTRACT

Osteosarcoma (OS) represents the most prevalent primary bone malignancy in dogs, and its growth and metastasis are highly dependent on angiogenesis. Gambogenic acid (GNA), a principal active component of the traditional Chinese medicine *Garcinia hanburyi*, has been demonstrated to possess broad-spectrum anti-tumor activity with low toxicity. Nevertheless, its effect on tumor angiogenesis in the canine OS has not yet been elucidated. This study aimed to investigate the effect of GNA on angiogenesis in the canine OS. The McKinley and Gracie canine OS cell lines were selected, and canine vascular endothelial cells (VECs) were isolated to establish an OS-VECs co-culture system. This system was used to evaluate the effects of GNA on the malignant behavior of OS cells and angiogenesis. Fibronectin Type III and SPRY Domain Containing 1 (FSD1) were overexpressed to investigate its role in canine OS cells and to determine whether it mediated the anti-tumor mechanisms of GNA. A subcutaneous xenograft tumor model was constructed in nude mice to validate the effects of GNA on tumor growth and angiogenesis. The results showed that GNA, with IC_{50} values of 0.28μM (McKinley) and 0.22μM (Gracie), inhibited the malignant behaviors and vasculogenic mimicry capacity of canine OS cells, and reduced the expression of several angiogenic factors. The microenvironment of GNA-treated canine OS cells suppressed the angiogenic capacity of VECs. Overexpression of FSD1 reversed the aforementioned anti-tumor effects of GNA. Gambogenic acid inhibited transplanted tumor growth, decreased microvessel density, and suppressed the expression of FSD1. In conclusion, this study found that GNA effectively inhibited the canine OS growth and angiogenesis by down-regulating FSD1, which supplemented the pharmacological mechanism of GNA anti-tumor activity.

To Cite This Article: Wang M, Zhang G, Sun J, Kang H, Li S, Wang W, Hou Q, Li P, Li X, Yang B, Fan H and Zhao Y, 2026. Gambogenic acid inhibits tumor angiogenesis and growth in canine osteosarcoma via fibronectin type III and spry domain containing 1 (FSD 1) modulation. Pak Vet J, 46(8): 1981-1994. http://dx.doi.org/10.29261/pakvetj/2026.190

INTRODUCTION

Osteosarcoma (OS) is the most common skeletal malignancy in medium- and large-breed dogs, with an incidence accounting for over 85% of all canine bone tumors (Lee and Loukopoulos, 2024). Canine OS is highly aggressive and exhibits a strong propensity for early pulmonary metastasis. Although surgery combined with adjuvant chemotherapy has prolonged the survival time of affected dogs to a certain extent, the toxic side effects and drug resistance associated with commonly used chemotherapeutic agents, such as *carboplatin* and *doxorubicin*, constitute major bottlenecks limiting therapeutic efficacy in treating this disease (Szewczyk *et al.*, 2015). Therefore, identifying highly effective and low-toxicity anti-OS drugs and therapeutic strategies represent critical issues that urgently need to be addressed in the field of veterinary clinical oncology. Canine OS is also recognized as a model for the human OS. Research in this area may therefore provide fresh insights that would benefit human patients as well.

Tumors cannot grow or spread without a blood supply, so angiogenesis is necessary for their progression (Al-Ostoot *et al.*, 2021). Inside the OS microenvironment,

cancer cells release a variety of pro-angiogenic factors that activate vascular endothelial cells (VECs), break down the basement membrane, and stimulate new vessel formation (Gola *et al.*, 2024). Canine OS can also form vasculogenic mimicry (VM) — channels built by tumor cells themselves that help feed the tumor (Massimini *et al.*, 2019). Higher microvessel density (MVD) has been linked to more invasive disease, and elevated Vascular Endothelial Growth Factor (VEGF) levels are tied to a shorter disease-free interval in affected dogs (Gola *et al.*, 2024). These connections have made angiogenesis a natural target for therapy. Drugs like bevacizumab, which blocks VEGF, have shown some benefit in human OS, but their long-term use is limited by their side effects and drug resistance (Liu *et al.*, 2021).

Gambogenic acid (GNA) is a natural compound extracted from gamboge, a resin secreted by *Garcinia hanburyi* plants native to south Asia (Hatami *et al.*, 2020). It belongs to the polycyclic pyranone family and well known for its strong anticancer effects, good stability, low toxicity, and relatively low cost (Sun *et al.*, 2018). Gambogenic acid has shown strong activity against a wide range of human cancers, including liver, gastric, and lung cancer. Its reported mechanisms include triggering apoptosis, disrupting the cell cycle (Mi *et al.*, 2024), and blocking tumor angiogenesis (Cheng *et al.*, 2018). Notably, researchers have developed GNA nanoparticles (CRNP-GNA) to enhance the therapeutic efficacy of GNA in targeting tumor vasculature (Du *et al.*, 2023). Additionally, GNA can increase the sensitivity of cancer cells to chemotherapy and reduce their resistance to multiple chemotherapeutic agents (Mi *et al.*, 2024). Thus, GNA holds broad research prospects in the field of anti-angiogenic tumor therapy; however, studies on GNA targeting angiogenesis in the Canine OS are lacking.

Fibronectin Type III and SPRY (SPla and Ryanodine Receptor) Domain-Containing 1 (FSD1) is a protein-coding gene located at the centrosome (Stein *et al.*, 2002). In glioblastoma (GBM), which is the most common, fastest-growing, most serious and aggressive type of primary malignant brain cancer, FSD1 restricts tumor cell dissemination and invasion by inhibiting histone deacetylase 6-mediated microtubule deacetylation (Xiao *et al.*, 2025). Furthermore, studies have indicated that elevated FSD1 expression levels are associated with decreased survival rates in patients with triple-negative breast cancer (Chen *et al.*, 2020). However, the expression, function, and regulatory mechanisms of FSD1 in OS remain unknown. The FSD1 is a key protein in cilium assembly, and its knockdown leads to defective ciliogenesis (Tu *et al.*, 2018). Several studies have revealed that ciliary defects lead to abnormal angiogenesis. (Xiong *et al.*, 2020; Pant *et al.*, 2025). Therefore, a potential link may exist between FSD1 and angiogenesis.

This study aimed to investigate whether GNA can modulate angiogenesis in the canine OS and to explore the underlying mechanisms, thereby further elucidating the pharmacological effects of GNA against canine OS, expanding the diagnostic and therapeutic horizons for canine OS in the veterinary field, while also expecting to provide significant comparative medicine implications for the treatment of human OS.

MATERIALS AND METHODS

Cell lines and cell culture: The canine OS cell lines McKinley and Gracie were kindly provided by the Flint Animal Cancer Center (Colorado State University, USA). Cells were cultured in high-glucose DMEM (Dulbecco's Modified Eagle's Medium) supplemented with 10% fetal bovine serum (Vivacell, Israel) and incubated at 37°C with 5% CO_2. Only Mycoplasma-negative cultures were used in all experiments. GNA (Shanghai Yuanye Bio-Tech, China) was supplied as a 10mM stock solution in DMSO. For in vitro experiments, the stock solution was diluted to the desired working concentrations using DMEM supplemented with 2% serum. The final DMSO concentration in all treatment groups was below 0.01%. An equivalent volume of DMSO at the same final dilution was added to all control groups.

Experimental animals and ethics statement: Twelve BALB/c nude mice aged 3 weeks and two Sprague-Dawley (SD) rats aged 6 weeks were procured from the Liaoning Changsheng Biotechnology Co., Ltd. and maintained under Specific Pathogen-Free (SPF) conditions at Northeast Agricultural University, Harbin, Heilongjiang, China. One healthy male Beagle dog (aged 7 months) was provided by the College of Veterinary Medicine, Northeast Agricultural University for the isolation of vascular endothelial cells (VECs). All procedures involving animals were conducted under protocols sanctioned by the Experimental Animal Research Ethics Committee of Northeast Agricultural University (SRM-11).

Isolation, culture, and identification of primary canine VECs: The cephalic vein (CV) and inferior vena cava (IVC) were aseptically isolated from an anesthetized Beagle dog. Vessels were digested with 0.1% type I collagenase. Harvested cells were maintained in Endothelial Cell Medium (ECM), as described earlier (Cai *et al.*, 2011) and characterized by immunofluorescence and transmission electron microscopy.

Cellular immunofluorescence assay: Cells were fixed and were permeabilized in 0.5% Triton X-100, blocked with 5% goat serum, and incubated overnight at 4°C with primary antibodies, followed by secondary antibody incubation. Nuclei were stained with DAPI (5μg/mL) and visualized under an inverted fluorescence microscope (Pan *et al.*, 2022).

Ultrastructural observation of cells: The samples underwent an initial fixation in 2.5% glutaraldehyde and were subsequently treated with osmium tetroxide. After gradient dehydration and infiltration, the cells were embedded and polymerized. Ultrathin sections (50–60nm) were prepared, stained, and observed under a transmission electron microscope (Hitachi, Japan), following Tavakolikazerooni *et al.* (2025).

Cell proliferation and toxicity assay: McKinley (5×10^3 cells/well) and Gracie (6×10^3 cells/well) cells were plated in 96-well plates and exposed to nine different concentrations (0.16, 0.20, 0.24, 0.28, 0.32, 0.36, 0.40, 0.44, and 0.48μM) of GNA for 48h. Cell viability was

assessed by adding 110μL of serum-free medium supplemented with 10% Cell Counting Kit-8 (CCK-8) solution (MeilunBio, China) to each well. Following a 3h incubation period at 37°C, optical density was recorded at 450nm. IC_{50} values were derived from the cell viability curves using nonlinear regression analysis (Wu *et al.,* 2023), and used as the dosing concentrations for subsequent experiments.

Colony formation assay: McKinley and Gracie cells were inoculated into 6-well plates at a concentration of 500 cells/well and subsequently maintained at 37°C with or without GNA for 10d. Following a PBS wash, the colonies were fixed using 4% paraformaldehyde for 15 min. After a second PBS rinse, the samples were treated with 0.1% crystal violet solution for 20 min, and finally rinsed with distilled water, air-dried, and imaged following the procedure of Jiang *et al.* (2022).

Transwell migration and invasion assays: McKinley and Gracie cells were resuspended in serum-free medium at a concentration of 5×10^4 cells/well and seeded into the upper chamber of Transwell inserts (Corning, USA), and incubated at 37°C for 24h with or without GNA. The bottom chambers were supplied with 600μL of DMEM supplemented with 20% serum. The co-cultured VECs were subsequently collected for Transwell migration assay under the same conditions. Following fixation, the migrated cells were stained using 0.1% crystal violet and subsequently visualized via microscopy. For the invasion assay, 60μL diluted Matrigel (Mogengel, China) was pre-coated on the upper chamber. The number of migrated or invaded cells was recorded from three randomly selected fields per insert following Wu *et al.* (2023).

Cell wound healing assay: McKinley and Gracie cells were plated in 12-well plates and allowed to reach confluence. A linear scratch was then introduced into the monolayer using a sterile 10μL pipette tip. After washing away detached cells, the remaining cells were incubated with or without GNA, and images were documented at 0, 6, and 12h. Wound area was quantified using ImageJ (Pan *et al.*, 2022).

Real-time PCR: RNA extraction was performed using the Eastep® Super RNA Extraction Kit, and cDNA was generated using the GoScript™ Reverse Transcription Kit (Promega, China). Using the Light Cycler® 480 II instrument (Roche, China) and 2×SYBR Green Master Mix (Bimake, China), amplification reactions were carried out. Gene expression was quantified using the $2^{-}\Delta\Delta Ct$ formula with GAPDH serving as the endogenous control (Zhao *et al.*, 2022). Primer details are provided in Table 1.

Western blotting: Total protein was isolated, run on SDS-PAGE, and blotted onto PVDF membranes. Blots were probed with primary antibodies (4°C, overnight) and secondary antibodies (room temperature, 2h). Bands were visualized with a gel imager and analyzed via ImageJ software, according to Zhao *et al.* (2022). Antibody information is provided in Table 2.

Tube formation assay: The bottoms of 24-well plates were covered with pre-chilled Matrigel and incubated at 37°C for 1h to ensure solidification. VECs from each co-culture group (1.5×10^5 cells/well) were seeded onto the Matrigel surface and incubated at 37°C for 6h. Tube formation was observed under an inverted microscope and photographed. Tubular structures were defined as closed, elongated networks connecting individual cells, and the number of complete tubes was counted from three randomly selected fields per well using ImageJ software (Prisco *et al.*, 2014).

Table 1: Primers used for real-time PCR

Gene	Accession Number	Product size (bp)	Primer sequences（5'-3'）
FSD1	XM_038429068.1	73	FCTTGTGCAAGATCTCCGGGC
			RCGAGAGGCTGGTAGTGATGAG
MMP2	XM_038659327.1	74	FTGTGGGACCACGGAAGACTA
			RCCAATAGTGGACATGGCGGT
VEGFA	NM_001003171455.3	145	FTTATCCAGGGCTTACCCTCCT
			RTTTGGGGAAGTAAAGGCGCA
HIF-1α	NM_001287163.1	138	FCCATTTTCCACCCAGGACACT
			RGCTCGCACTTTGAGGACTTG
ANGPT-1	XM_038684521.1	139	FCTCATGCTAACAGGAGGCTG
			RGTAAGGAGTAACTGGGCCCTT
ANGPT-2	NM_001048127.6	79	FTCCACAGAGGAGATAAAGGATTCAC
			RTCCTGGTTGGCTTATGCTGC
GAPDH	NM_001003141.2	150	FTGCCTCCTGCACCACCAAC
			RCCGTCACGCCACATCTTCCC

Table 2: Primary antibody sources for Western blotting

Antibody name	Source	Dilution ratio
FSD1	124848, Zenbio, USA	1:1000
MMP2	C12L21, Selleck, China	1:1000
VEGFA	G24N11, Selleck, China	1:500
HIF-1α	WL01508, Wanleibio, China	1:1000
ANGPT-1	G8C23, Selleck, China	1:1000
ANGPT-2	M10L24, Selleck, China	1:10000
GAPDH	60004-1-Ig, Proteintech, USA	1:50000

Aortic ring sprouting assay: Thoracic aortas from SD rats were sectioned into 1mm rings, digested in 2g/L type II collagenase until the outer membrane becomes loose. These digested rings were then embedded in Matrigel, and cultured with CM mixed with VEC complete medium, and incubated at 37°C for 7d. Sprouting was observed and counted (Baker *et al.*, 2011).

Subcutaneous xenograft model: Nude mice were randomized into GNA and control groups (n = 6/group), and acclimatized for 7 days prior to tumor inoculation. Gracie cells (1×10^7 cells per mouse) in a PBS-Matrigel mixture were injected subcutaneously into the right axilla of nude mice in the control and GNA groups. GNA (4mg/kg), dissolved in a vehicle containing 1% DMSO, 10% PEG300, 5% Tween-80, and 84% 0.9% NaCl, was injected intraperitoneally every 2 days for 48 days; the CON group received the vehicle alone. Tumor growth was monitored every 6 days via digital caliper measurements, and volumes were computed as $(\text{length}\times\text{width}^2)/2$. At the study endpoint (day 48), mice were euthanized, and the tumors were resected, weighed, and imaged. Tumor volume measurement and tumor weighing were performed by investigators blinded to the treatment group allocation.

Immunohistochemical staining: Tumor tissues underwent fixation, dehydration, embedding, sectioning, deparaffinization, rehydration, and antigen retrieval. The slides were treated with primary antibodies against CD31, VEGFA, and FSD1 (overnight, 4°C) and subsequently exposed to biotinylated secondary antibodies at room temperature. Visualization was achieved using a DAB

substrate kit, followed by hematoxylin counterstaining. Images were observed and scanned under microscope (Novikova *et al.*, 2016). For CD31 staining, microvessel density (MVD) was assessed by manually counting CD31-positive vessels in three randomly selected high-power fields (×200 magnification) per section, and the MVD value for each sample was calculated as the average count across the three fields. For VEGFA and FSD1 staining, the H-score method was used. Staining intensity was scored as 0 (negative), 1 (weak), 2 (moderate), or 3 (strong), and the percentage of cells at each intensity level was estimated in three randomly selected fields (×200 magnification) per section. The H-score was calculated as: H-score = (1×% weak) + (2×% moderate) + (3×% strong), yielding a range of 0–300. For visual consistency with the CD31 data, the H-score values were normalized to the CON group and presented as relative staining strength. Data quantification was conducted by two independent investigators who were blinded to the experimental conditions.

FSD1 overexpression: FSD1 overexpression and negative control plasmids (Shanghai GeneChem Co., Ltd.) were transfected into McKinley and Gracie cells using E-trans reagent. McKinley and Gracie cells were seeded into 6-well plates. When the cell density reached approximately 80%, the plasmids, E-trans, and transfection reagent (Shanghai GeneChem Co., Ltd.) were added at the appropriate ratios according to the manufacturer's instructions. After 6h, the transfection medium was discarded and replaced with fresh culture medium (Yang *et al.,* 2017).

Statistical analysis: Data normality was assessed using the Shapiro-Wilk test for datasets with n=6. All data are expressed as mean ± SD. For comparisons between two groups, an independent sample t-test was used. For comparisons among three or more groups, one-way ANOVA followed by Tukey's post hoc test was applied. All statistical analyses were performed using GraphPad Prism 10.

RESULTS

GNA inhibits the malignant behaviors of canine OS cells: The results of the CCK-8 assay showed that GNA inhibited the proliferative activity of both canine OS cells lines in a dose-dependent manner (Fig. 1A). The IC_{50} values of GNA were determined to be 0.28μM for McKinley cells and 0.22μM for Gracie cells, and these concentrations were used as the GNA doses for the treatment groups in subsequent experiments. After treatment with GNA, McKinley and Gracie cells clonogenesis (Fig. 1B), migration (Fig. 1C-D), and invasion (Fig. 1E) decreased (P<0.05).

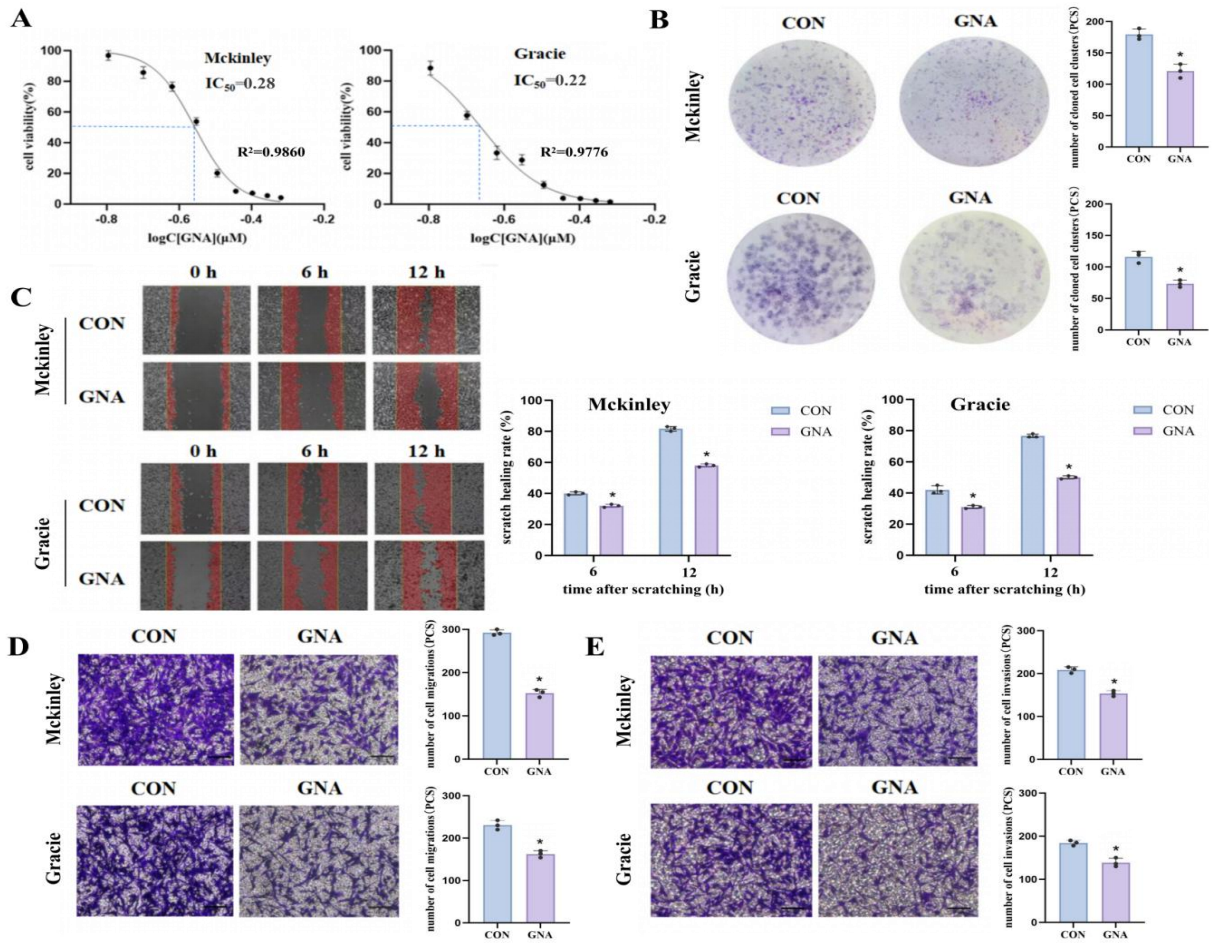

Fig. 1: Effect of GNA on malignant biological behaviors of canine OS cells. CCK-8 assay for the viability of canine OS cells. GNA concentrations are presented on a logarithmic scale for clarity of dose–response visualization. (B) Representative images of plate colony formation and data analysis charts. (C) Representative images of wound healing assay captured at 0, 6, and 12h after scratching, and data analysis charts. (D) Representative images of Transwell migration assays and data analysis charts. (E) Representative images of Transwell invasion assays and data analysis charts. All scale bars in this image series: 150μm. *P<0.05 versus CON group.

Isolation, culture, and identification of canine VECs: Two types of VECs were obtained from canine veins: VECs derived from the cephalic vein (CV VECs) and VECs derived from the inferior vena cava (IVC VECs). After 4 days, both colonies that formed expanded into a confluent cobblestone monolayer by day 8 (Fig. 2A). CCK-8 assays confirmed stable proliferation upon passaging (Fig. 2B), and transmission electron microscopy revealed Weibel-Palade bodies, a defining feature of endothelial cells, in both cell types (Fig. 2C). Cellular immunofluorescence staining showed that both VEC types were positive for the endothelial cell-specific antigen CD31, with CD31 positivity rates of 98.11 and 98.87% for CV VECs and IVC VECs, respectively (Fig. 2D). Collectively, two high-purity, stably passaged canine VEC models were successfully obtained for subsequent co-culture experiments.

GNA inhibits tumor angiogenesis in canine OS in vitro: The effects of GNA on the expression of angiogenic factors in canine OS cells were examined by qRT-PCR and Western blot. The results showed that the mRNA (Fig. 3A) and protein expression levels (Fig. 3B) of ANGPT-1, ANGPT-2, MMP-2, VEGFA, and HIF-1α in both McKinley and Gracie cells were significantly decreased ($P<0.05$) following GNA treatment. The tube formation assay demonstrated that both McKinley and Gracie cells exhibited VM, and GNA significantly inhibited ($P<0.05$) the VM of both cell lines (Fig. 3C). At IC_{50} concentrations of 0.28 and 0.22μM, GNA did not markedly reduce VEC viability, which stayed above 95% (Fig. 4A), suggesting low direct toxicity. To examine the effect of GNA on endothelial cells within the tumor microenvironment, two models, a Transwell co-culture system and a conditioned medium model, were established (Fig. 4B). The results showed that, compared with the CON group, the cell viability (Fig. 4C), migration (Fig. 4D), and tube formation (Fig. 4E) abilities of both CV VECs and IVC VECs co-cultured with GNA-treated canine OS cells were decreased ($P<0.05$). Conditioned medium collected from GNA-pretreated tumor cells was applied to rat aortic rings. GNA attenuated ($P<0.05$) the ability of canine OS cells to induce aortic ring sprouting (Fig. 4F).

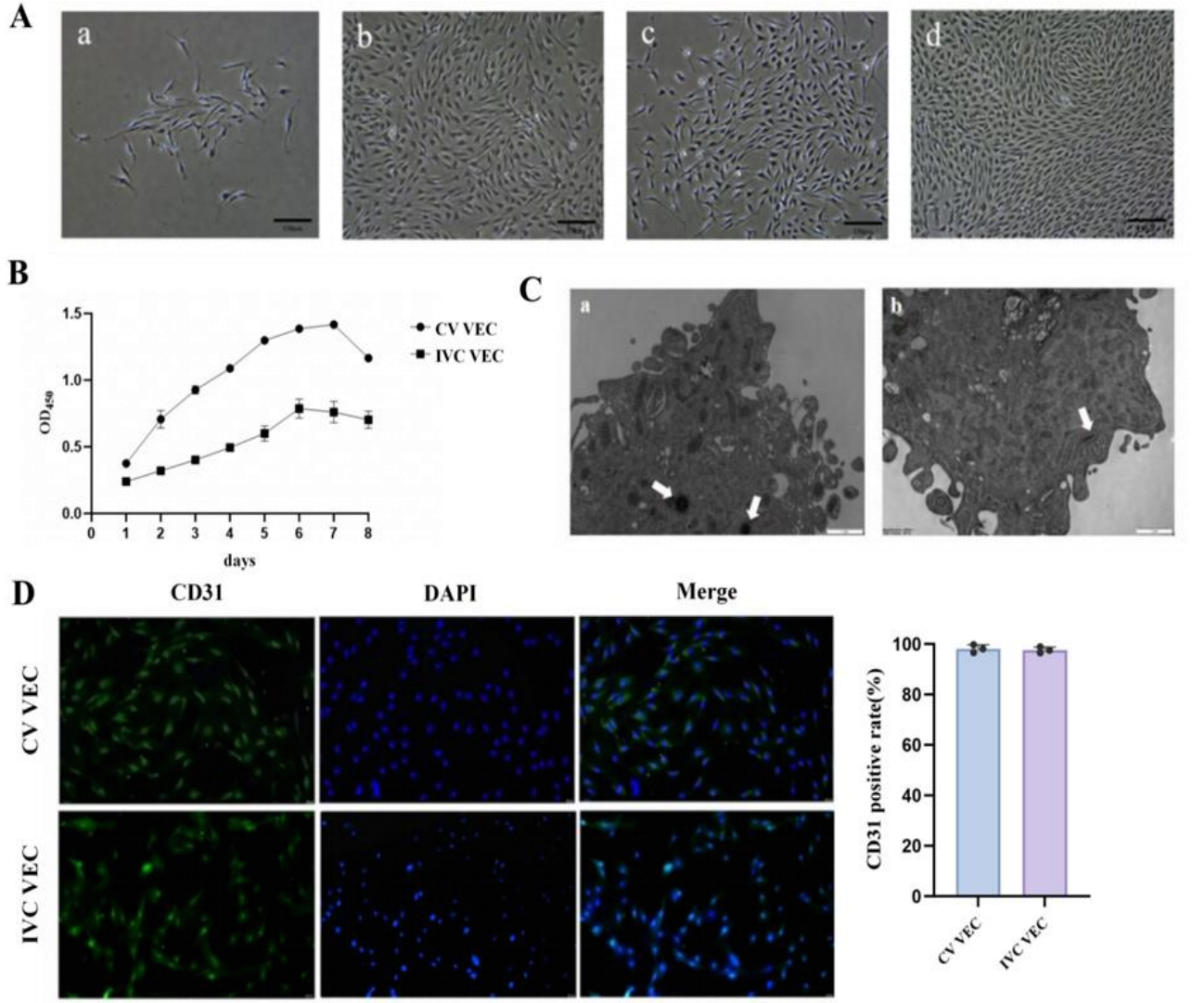

Fig. 2: Results of canine VEC isolation and identification. (A) Morphology of primary canine VECs. a and b respectively show the morphology of primary CV VECs after 4d and 8d of culture; c and d respectively show the morphology of IVC VECs after 4d and 8d of culture. Scale bar: 150μm. (B) Growth curve of two types of VECs after subculture. (C) Identification results of VECs by transmission electron microscopy. White arrows indicate Weibel-Palade bodies. a and b show the ultrastructure of CV VECs and IVC VECs. Scale bar: 1μm. (D) Immunofluorescence assay results and data analysis charts. Scale bar: 20μm.

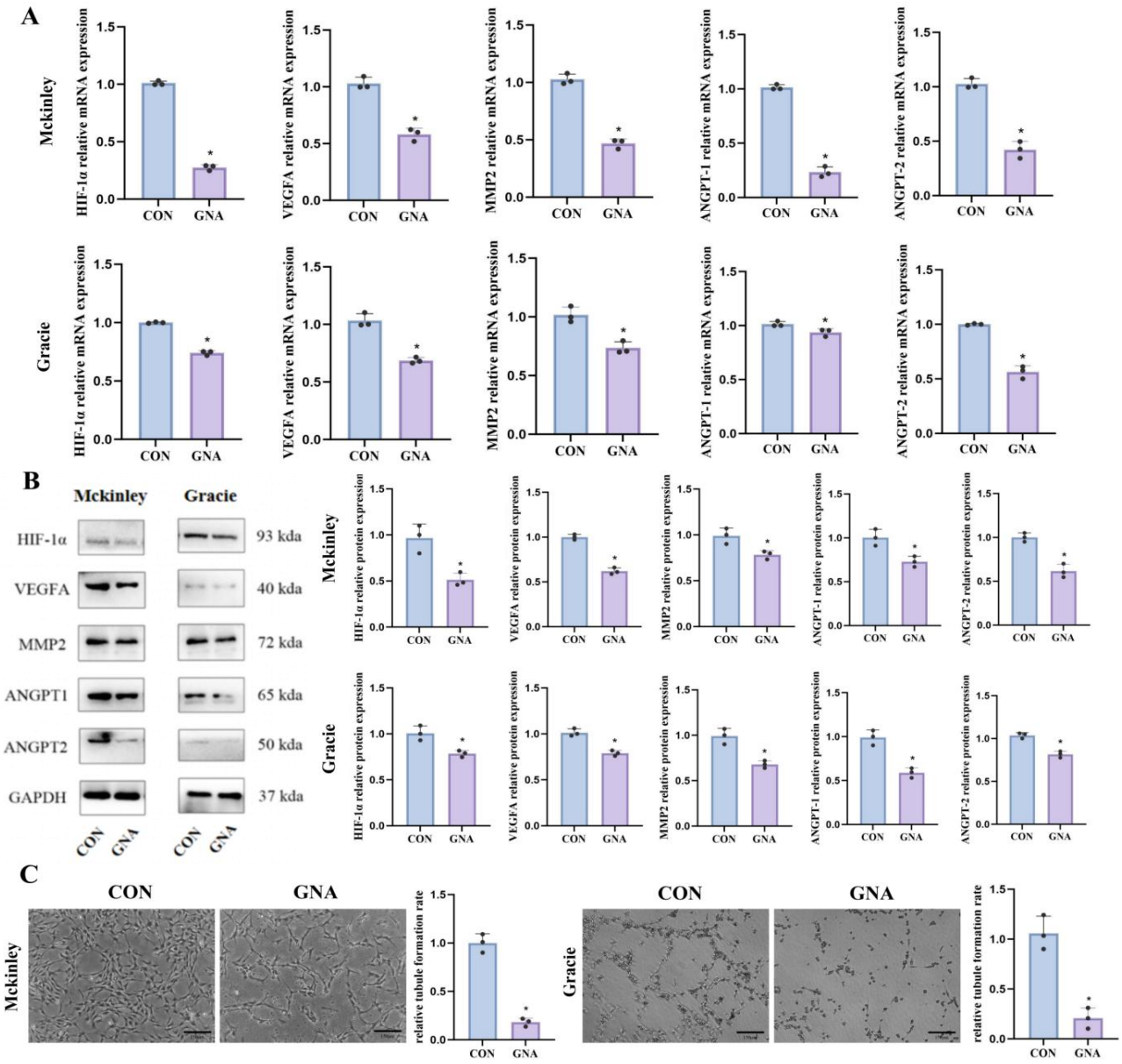

Fig. 3: Effects of GNA on in vitro tumor angiogenesis in canine OS. (A) mRNA expression changes of angiogenic factors in McKinley and Gracie cells. (B) Protein expression changes of angiogenic factors in McKinley and Gracie cells. (C) VM formation capacity changes of McKinley and Gracie cells. Scale bar: 150μm. *P<0.05 versus CON group.

FSD1 reversed the inhibitory effect of GNA on the malignant behaviors of canine OS cells: The qRT-PCR and Western blot analysis showed that GNA treatment significantly reduced (P<0.05) the mRNA (Fig. 5A) and protein expression (Fig. 5B) of FSD1 in both McKinley and Gracie cells. To further explore the role of FSD1 in the antitumor effects of GNA in vitro, transient FSD1 overexpression models (oeFSD1) were constructed in McKinley and Gracie cells, with a negative control (NC) group established in parallel. The experiment included four groups: NC, NC+GNA, oeFSD1, and oeFSD1+GNA. The results showed that oeFSD1 promoted (P<0.05) the cell viability (Fig. 5C), colony formation (Fig. 5D), migration (Fig. 5E-F), and invasion (Fig. 5G) abilities of both McKinley and Gracie cells, and reversed (P<0.05) the inhibitory effects of GNA on these capacities.

FSD1 reversed the inhibitory effect of GNA on angiogenesis in canine OS cells: qRT-PCR results showed that, compared with the NC group, the mRNA expression levels of ANGPT-2, MMP-2, VEGFA, and HIF-1α were upregulated (P<0.05) in the oeFSD1 group in both McKinley and Gracie cells; however, the mRNA expression of ANGPT-1 exhibited opposite trends in the two cell lines following oeFSD1. Moreover, compared with the NC+GNA group, oeFSD1 reversed (P<0.05) the inhibitory effect of GNA on the mRNA expression of these factors in both canine OS cell lines, as shown in the oeFSD1+GNA group (Fig. 6A). Western blot results demonstrated that oeFSD1 increased (P<0.05) the protein expression levels of ANGPT-1, ANGPT-2, MMP-2, VEGFA, and HIF-1α in both canine OS cell lines and markedly reversed the inhibitory effect of GNA on the protein expression of these factors (Fig. 6B). The tube formation assay indicated that oeFSD1 significantly promoted the tube-forming capacity of both canine OS cell lines and (P<0.05) reversed the inhibitory effect of GNA on this capacity (Fig. 6C).

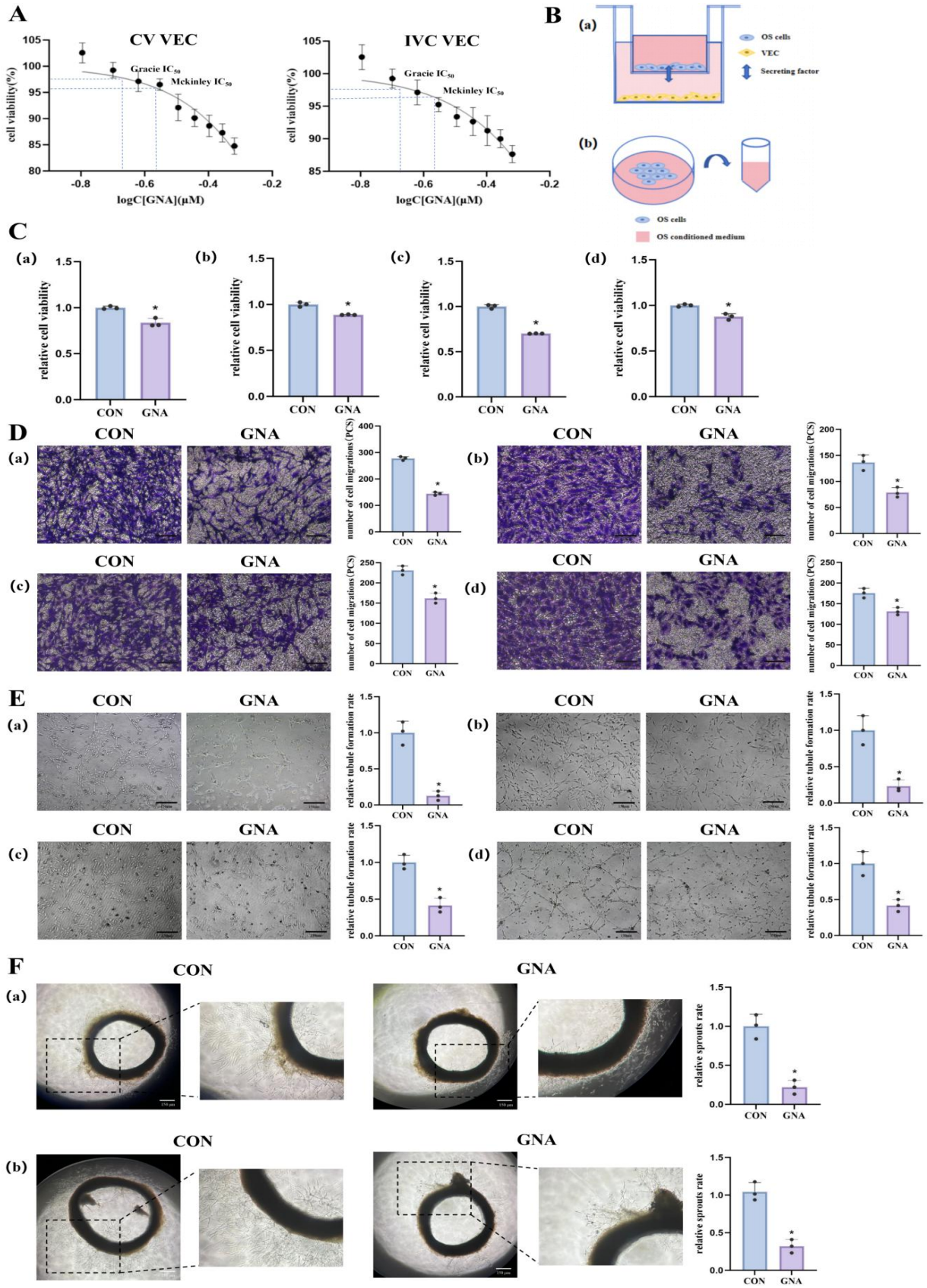

Fig. 4: Effects of GNA on in vitro tumor angiogenesis in canine OS. (A) CCK-8 assay for the viability of canine VECs. (B) Schematic diagram of the co-culture system of canine OS cells and canine VECs. (a) Schematic diagram of indirect co-culture using Transwell inserts. OS cells in the upper chamber were treated with GNA for 48h, after which the upper inserts were removed and the bottom-layer VECs were collected for functional assays; (b) Schematic diagram of tumor conditioned medium preparation. OS cells were treated with GNA for 48h, washed twice with PBS, and incubated in fresh serum-free medium for an additional 24h. The supernatant was then collected as CM. (C) CCK-8 assay for the viability of canine VECs after co-culture. (D) Representative images of Transwell migration assays and data analysis charts. (E) Representative images of tube formation assays and data analysis charts. For (C), (D), and (E): (a), (b) CV VECs co-cultured with McKinley and Gracie cells; (c), (d) IVC VECs co-cultured with McKinley and Gracie cells. (F) Representative images of rat aortic ring sprouting assays and data analysis charts. (a), (b) Experimental results and analysis after intervention with McKinley and Gracie conditioned medium. All scale bars in this image series: 150μm. *P<0.05 versus CON group.

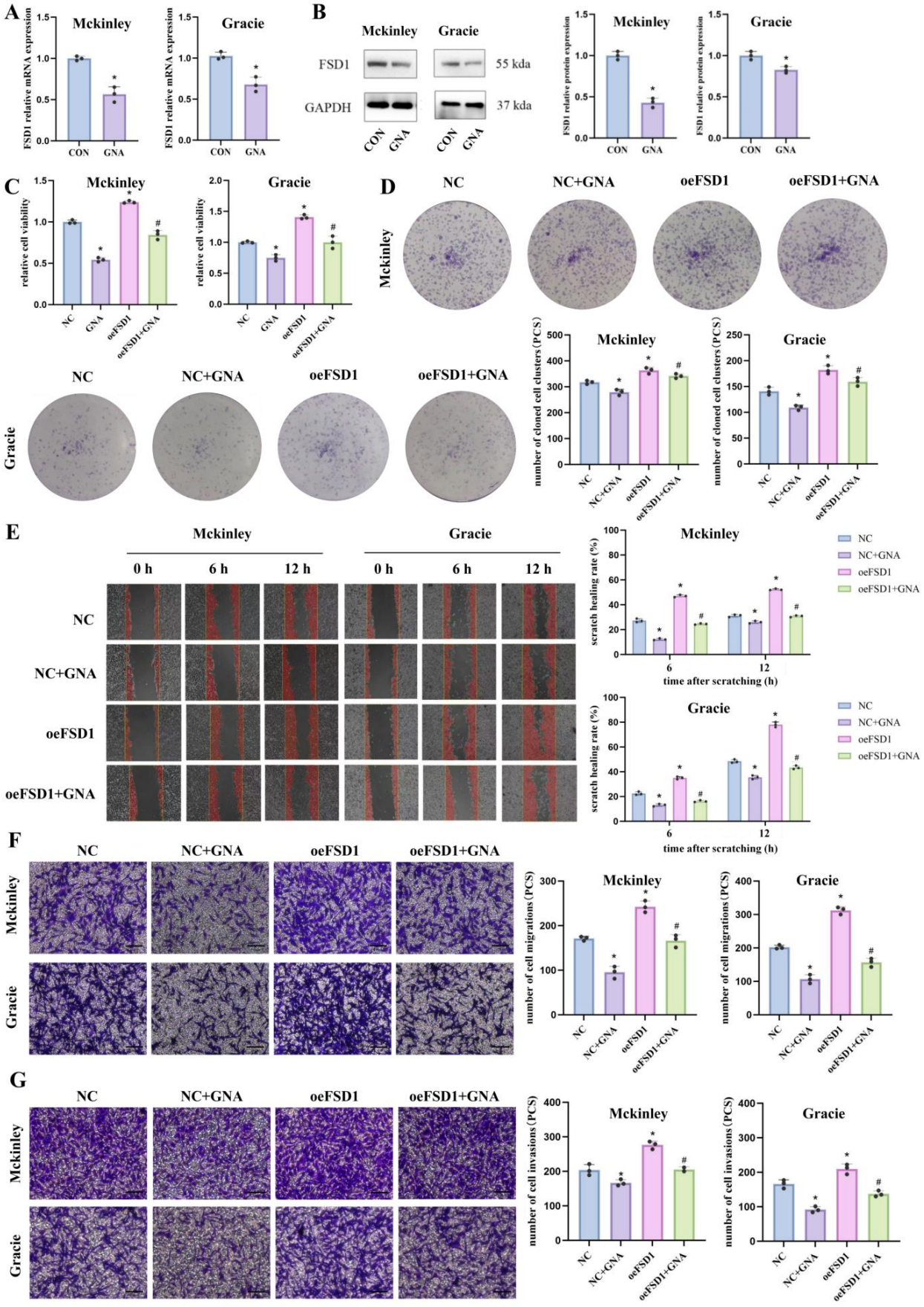

Fig. 5: Effects of FSD1 on GNA-mediated inhibition of malignant behaviors in canine OS cells. (A) mRNA expression changes of FSD1 in McKinley and Gracie cells. (B) Protein expression changes of FSD1 in McKinley and Gracie cells. (C) CCK-8 assay for the viability of canine OS cells. (D) Representative images of plate colony formation and data analysis charts. (E) Representative images of wound healing assay and data analysis charts. (F) Representative images of Transwell migration assays and data analysis charts. (G) Representative images of Transwell invasion assays and data analysis charts. All scale bars in this image series: 150μm. *P<0.05 versus NC group. #P<0.05 versus NC+GNA group.

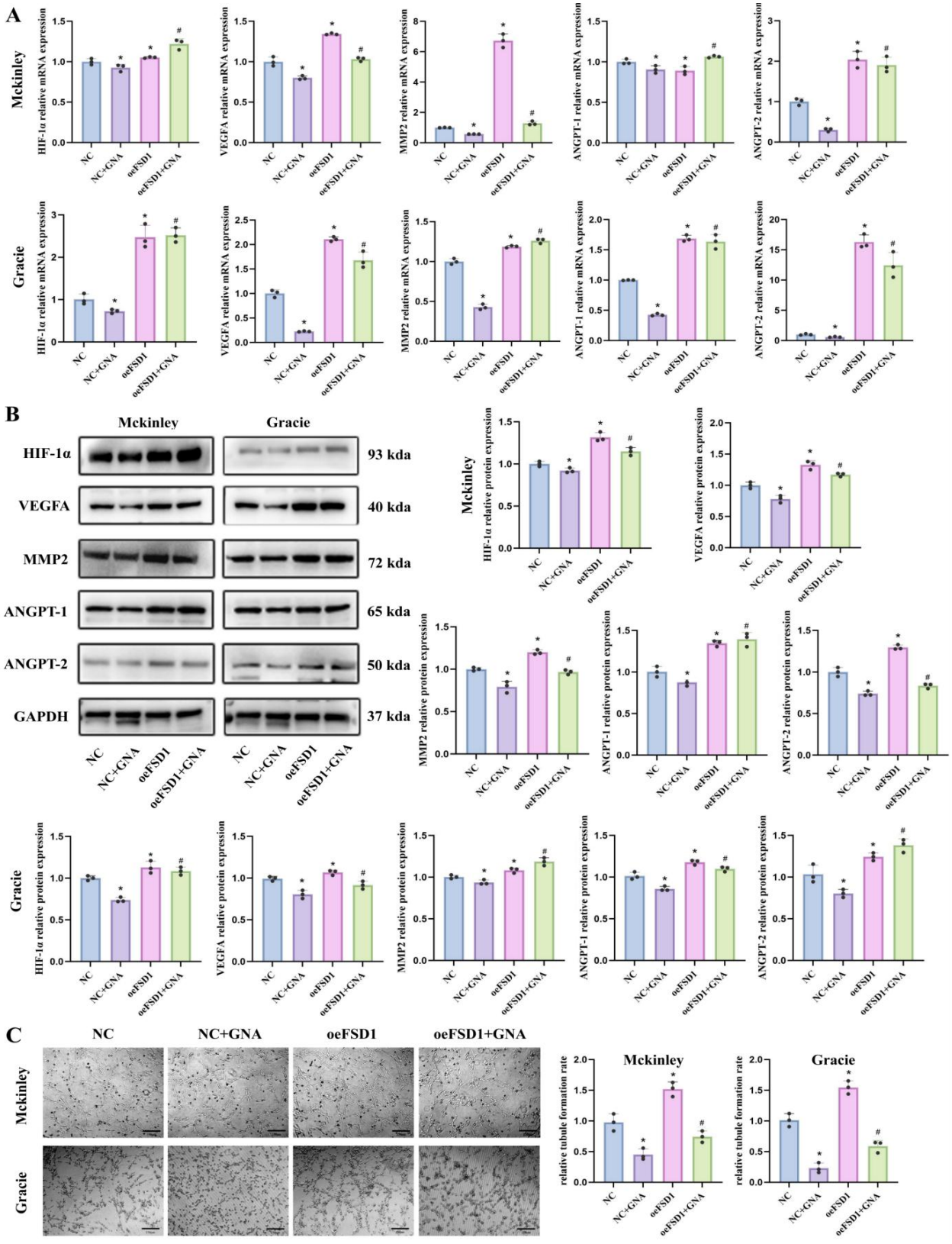

Fig. 6: Effect of FSD1 on GNA-mediated inhibition of angiogenesis in canine OS cells. (A) mRNA expression changes of angiogenic factors in McKinley and Gracie cells. (B) Protein expression changes of angiogenic factors in McKinley and Gracie cells. (C) VM formation capacity changes of McKinley and Gracie cells. Scale bar: 150μm. *P<0.05 versus NC group. #P<0.05 versus NC+GNA group.

The results showed that, compared with the NC group, the cell viability (Fig. 7A), migration (Fig. 7B), and tube formation (Fig. 7C) abilities of both CV VECs and IVC VECs co-cultured with oeFSD1 canine OS cells were enhanced (P<0.05). Moreover, compared with the NC+GNA group, the inhibitory effects of GNA on these abilities were reversed (P<0.05) in the oeFSD1+GNA group. Conditioned medium from each group was collected and applied to rat aortic rings. It was seen that oeFSD1 significantly enhanced the ability of canine OS cells to induce aortic ring sprouting and reversed (P<0.05) the inhibitory effect of GNA on this ability (Fig. 7D).

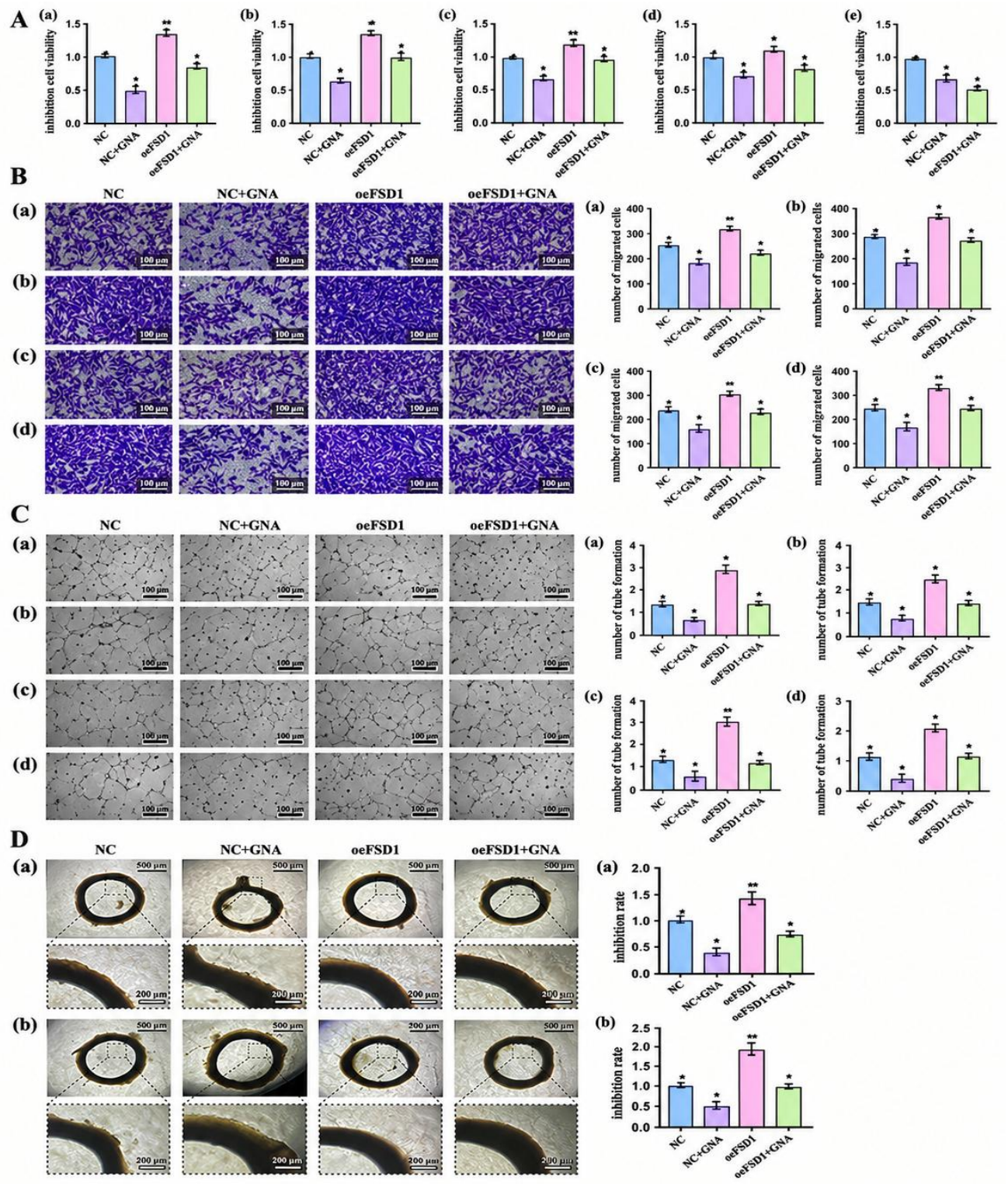

Fig. 7: Effect of FSD1 on GNA-mediated inhibition of angiogenesis in canine OS cells. (A) CCK-8 assay for the viability of canine VECs after co-culture. (B) Representative images of Transwell migration assays and data analysis charts. (C) Representative images of tube formation assays and data analysis charts. For (A), (B), and (C): (a), (b) CV VECs co-cultured with McKinley and Gracie cells; (c), (d) IVC VECs co-cultured with McKinley and Gracie cells. The corresponding quantitative data for panels (a), (b), (c), and (d) are presented in panels (ai), (bi), (ci), and (di), respectively. (D) Representative images of rat aortic ring sprouting assays and data analysis charts. (a), (b) Experimental results and analysis after intervention with McKinley and Gracie conditioned medium. All scale bars in this image series: 150μm. *P<0.05 versus NC group. #P<0.05 versus NC+GNA group.

GNA inhibits tumor growth and angiogenesis in canine OS *in vivo*: The mean tumor weight in the GNA group was significantly lower than that in the CON group at the end of the modeling period (Fig. 8A). During the modeling period, the growth rate of subcutaneous xenograft tumors in nude mice in the GNA group was markedly slower than that in the CON group (Fig. 8B). Notably, non-significant difference in body weight was observed between the GNA group and the control group (Fig. 8C), indicating that GNA did not affect body weight gain in nude mice. Immunohistochemical staining showed that the GNA group exhibited a significant reduction in tumor MVD and markedly decreased expression levels of VEGFA and FSD1 (Fig. 8D).

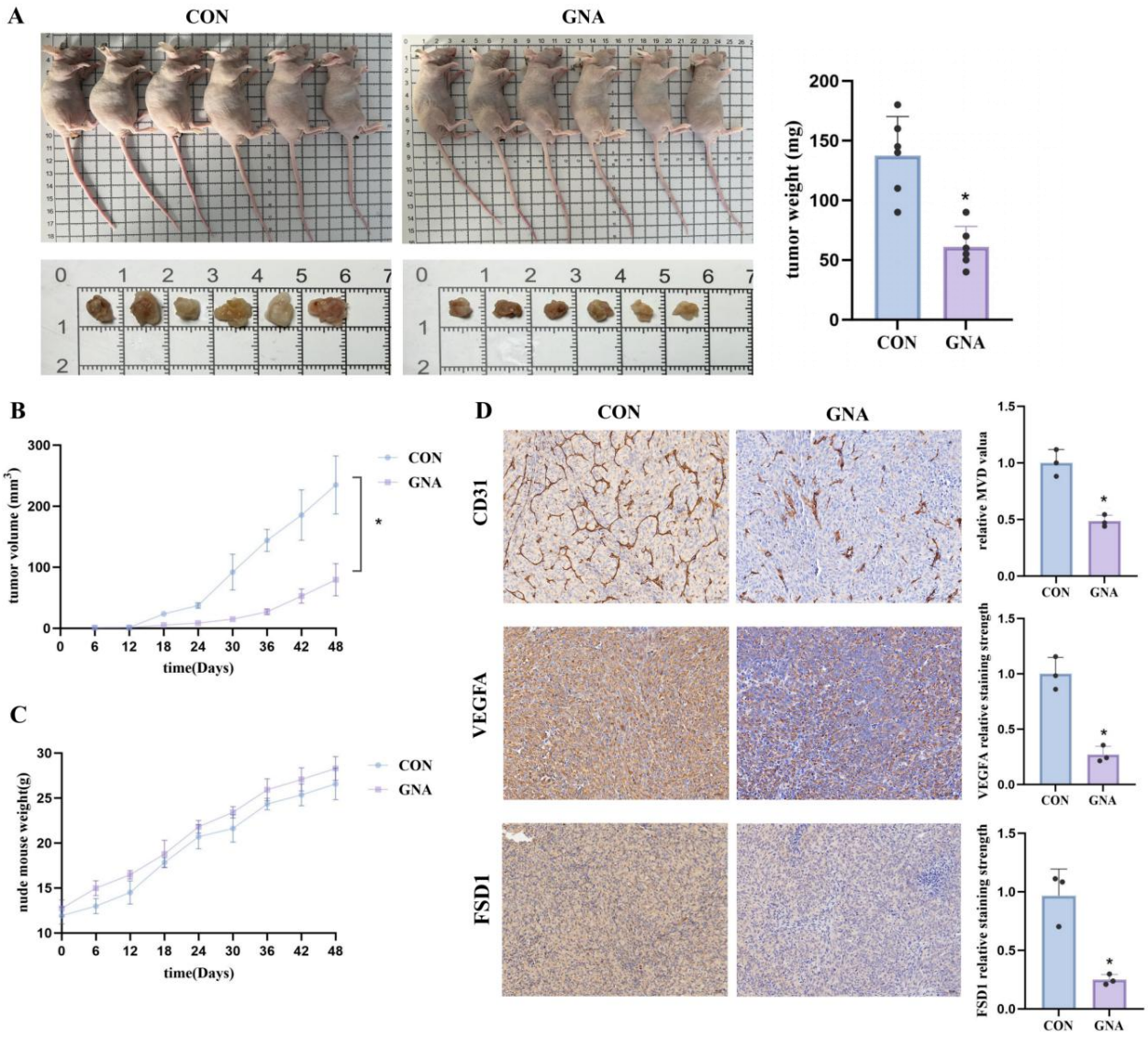

Fig. 8: Effects of GNA on the growth and angiogenesis of canine OS xenograft tumors. (A) Xenograft tumor size and weight at the end of the modeling period. Tumors were photographed on a measurement board with scale markings in centimeters (small divisions=1 mm; large divisions=1 cm). (B) Tumor growth curves. (C) Body weight growth curves of nude mice. (D) Representative images of immunohistochemical staining and data analysis charts (200×). Scale bar: 50μm. *P<0.05 versus CON group.

DISCUSSION

Canine osteosarcoma (OS) is the predominant form of primary bone cancer in dogs. Despite the current standard of care combining amputation with high-dose postoperative chemotherapy, the median survival of dogs with OS remains under 12 months (Lee and Loukopoulos, 2024). Natural products have drawn interest in the development of drugs for cancer treatment because they often show good efficacy with relatively low toxicity. Gambogenic acid (GNA) is a flavonoid that selectively suppresses the growth of multiple cancer cell types, offering broader activity and a better safety profile than related compounds like gambogic acid (Sun *et al.*, 2018). In the present study, GNA markedly inhibited the malignant behavior of canine OS cells with IC_{50} values of 0.28μM (McKinley) and 0.22μM (Gracie). For comparison, natural compounds such as sulforaphane have also shown activity against canine OS cells, with reported IC_{50} values of 37.5μM (D17) and 18.3μM (OS2.4) (Rizzo *et al.*, 2017), indicating a substantially lower effective concentration of GNA. A recent study has shown that GNA had very low toxicity toward canine MDCK kidney cells, with cell survival remaining at 93.33% after treatment with 0.28μM GNA (Li *et al.*, 2025). Likewise, GNA caused minimal damage to normal tissues in a mouse prostate cancer model (Wu *et al.*, 2022). In terms of pharmacokinetics, the plasma half-life of GNA in dogs following intravenous administration of 1mg/kg was 141.74±7.92min (Chen *et al.*, 2014), which is substantially longer than that of antitumor agents such as paclitaxel (2.5mg/kg, intravenous), reported to be 30.6±10.8min in female dogs and 21.6±10.8min in male dogs (Liu *et al.*, 2014). Together, properties, such as strong antitumor activity, low toxicity, and favorable pharmacokinetics, make GNA a promising candidate for OS therapy.

From a translational perspective, the IC_{50} values of GNA (0.22–0.28μM) determined in this study are substantially lower than the maximum plasma concentration (~9.01μM) achieved in dogs following intravenous administration of GNA at 1mg/kg (Chen *et*

al., 2014). While direct extrapolation from in vitro IC_{50} values to in vivo efficacy must be interpreted with caution, this comparison provides a preliminary indication that pharmacologically relevant concentrations of GNA may be achievable in vivo. Using the FDA body surface area-based dose conversion method, the 4mg/kg mouse dose used in our xenograft model corresponds to a canine equivalent dose of approximately 0.6mg/kg, which is within a range comparable to the 1 mg/kg dose previously evaluated in dogs without severe toxicity (Chen *et al.*, 2014). These observations suggest that GNA may possess a favorable therapeutic window, although dedicated dose-escalation and toxicity studies in dogs are required to confirm its clinical applicability.

Canine OS mostly relies on abundant blood vessels for its growth and metastasis, so angiogenesis plays the most important role in its biology (Gola *et al.*, 2024). Yet effective anti-angiogenic therapies are not available. This study showed that GNA lowered the expression of VEGFA, HIF-1α, MMP-2, ANGPT-1, and ANGPT-2 simultaneously. VEGF, in particular, is a key driver of vessel formation in OS and is strongly associated with the tumor aggressiveness and prognosis (Gola *et al.*, 2024). Hypoxia within the OS microenvironment activates HIF-1α, which in turn upregulates VEGF (Gola *et al.*, 2020) and ANGPT-2 (Xu and Tang, 2024). The significant inhibition of HIF-1α by GNA observed in the present study may therefore partially account for the concurrent downregulation of VEGFA and ANGPT-2. These results suggest that GNA may coordinately suppress multiple pro-angiogenic factors, at least in part, through the modulation of basal HIF-1α levels, a notion partially consistent with the findings of Xun *et al.* (2024). Whether GNA also affects HIF-1α expression under true hypoxic conditions remains to be investigated in future studies. ANGPT1 stabilizes mature vasculature through TIE2 activation (Fagiani *et al.*, 2011); its partial suppression by GNA implies that GNA may disrupt existing tumor vessels in addition to inhibiting neovascularization. The MMP-2 is highly expressed in OS and correlates with its malignancy and poor prognosis (Gao *et al.*, 2023). Downregulation of MMP-2 by GNA recorded in this study suggests that GNA may reduce extracellular matrix degradation, thereby impeding VEC recruitment toward tumor cells. Importantly, while clinically used anti-angiogenic agents such as bevacizumab, sunitinib, and sorafenib are associated with limited efficacy and various adverse effects including hypertension, hemorrhages, and cardiotoxicity (You *et al.*, 2023), GNA exhibited favorable safety; with IC_{50} values of 0.28μM (McKinley cell line) and 0.22μM (Gracie cell line), viability of both canine primary VECs types remained above 95%, indicating that GNA preserves a meaningful safety margin toward normal vasculature while exerting potent anti-angiogenic effects.

Besides five angiogenic factors (VEGFA, HIF-1α, MMP-2, ANGPT-1, and ANGPT-2), tumor angiogenesis can also depend on other factors. Therefore, a thorough evaluation of anti-angiogenic activity calls for multiple experimental approaches. In this study, both VM assays and OS-VEC co-culture systems were used to examine the anti-angiogenic effects of GNA. Gambogenic acid (GNA) suppressed VM formation in canine OS cells and, impaired the proliferation, migration, sprouting, and tube formation of VECs in a co-culture setting that mirrors the tumor microenvironment. A particular strength of the experimental design was the use of primary canine VECs instead of the standard human umbilical vein endothelial cells, yielding a fully homologous system that avoids species-mismatch artifacts. As VECs from distinct anatomical origins may differ phenotypically and functionally (Aranguren *et al.*, 2013), two types of canine primary VECs (derived from the CV and IVC) were isolated; their concordant responses to GNA treatment further supported the generality of our findings. This homologous platform also served as a reliable *in vitro* model for future canine OS angiogenesis research. Consistent with the established association between elevated MVD and high-grade OS (Gola *et al.*, 2024), GNA significantly reduced tumor MVD and VEGFA expression *in vivo*, corroborating its anti-angiogenic efficacy.

Of note, FSD1 has been reported to exert opposing roles in different tumor types—tumor-suppressive in glioblastoma (Xiao *et al.*, 2025) and oncogenic in breast cancer (Chen *et al.*, 2020)—highlighting the context-dependent nature of its function and the necessity of investigating FSD1 specifically in OS. The results of the present study indicate that FSD1 promotes malignant behaviors in two canine OS cell lines, providing a reference for exploring the functional role of FSD1 in canine OS. Based on existing research, mechanistic speculation regarding whether FSD1 regulates angiogenesis may have been limited to its influence on endothelial cell cilia. However, from a structural biology perspective, FSD1 contains both the SPRY domain and a fibronectin type III (FNIII) domain. In glioblastoma, upregulated SPRY2 expression is associated with poor patient prognosis and promotes tumor growth and angiogenesis by maintaining the tumorigenic capacity of tumor stem cells and inducing VEGF expression (Park *et al.*, 2017). Concurrently, the expression level of tenascin-C, which contains FNIII domains, is positively correlated with WHO grade and promotes VM formation through its EGF-like domain (Chen *et al.*, 2024). In conjunction with the findings of the present study that FSD1 overexpression significantly reversed the inhibitory effect of GNA on the five angiogenic factors in both canine OS cell lines, it can be inferred that FSD1 may reside upstream within the regulatory network of the aforementioned five angiogenic factors, thereby exerting a regulatory effect on angiogenesis in canine OS. The precise molecular link between FSD1, a centrosome-localized protein, and the transcriptional regulation of angiogenic factors remains to be fully elucidated.

The translational relevance of our findings based on the canine OS model to human OS warrants further investigation. Canine OS shares key features with its human counterpart in biology, molecular mechanisms, and drug response, making it a useful comparative model (Romanucci *et al.*, 2023). Unlike conventional xenograft models, canine OS model is characterized by spontaneous onset, intact immune system, and fast progression features that allow drug testing in a more relevant tumor environment (Romanucci *et al.*, 2023). In such models, tumors grow in immunocompetent hosts under natural

conditions, offering a more faithful readout of therapeutic effects. Previous studies have shown that GNA blocks OS cell proliferation via the USP9x/SOX2 pathway (Chen *et al.*, 2020). Together with this work and the recent report by Li *et al.* (2025), the cumulative evidence suggests that GNA exhibits activity against OS across species, making it an attractive candidate for joint veterinary and human drug development.

Several avenues warrant further investigation. First, the molecular mechanism by which FSD1 regulates angiogenic factor expression remains to be defined. Elucidating whether FSD1 interacts with specific transcription factors or co-activators will require Co-IP coupled with mass spectrometry to identify FSD1-interacting proteins, combined with ChIP-seq to delineate its downstream transcriptional network. Second, while this study focused on FSD1 function in canine OS cells, its expression changes in tumor-derived VECs and its impact on tumor vascular structure and function deserve further exploration. Third, the primary canine VECs used in this study were isolated from a single Beagle dog, and biological variability among individual donors was not captured. Although two distinct VEC populations from different anatomical sites (CV and IVC) showed consistent results, future validation using cells from multiple independent donors is warranted. Additionally, these primary VECs have limited passage capacity, and the establishment of immortalized cell lines would facilitate long-term investigations. Finally, the expression profile of FSD1 in clinical canine OS specimens and its correlation with patient prognosis should be validated through the use of relevant tissue.

Conclusions: Gambogenic acid (GNA), at its IC_{50} concentrations of 0.28μM for McKinley cells and 0.22μM for Gracie cells, inhibited the malignant behaviors and vasculogenic mimicry, and downregulated the expression of five angiogenesis-related factors in canine OS cells, including ANGPT-1, ANGPT-2, MMP-2, VEGFA, and HIF-1α. It also suppressed the angiogenic capacity of VECs within the tumor microenvironment. Overexpression of FSD1 significantly reversed the above-mentioned anti-tumor effects of GNA. Furthermore, GNA inhibited xenograft tumor growth and angiogenesis *in vivo*. These findings identify FSD1 as a key mediator of the anti-osteosarcoma effects of GNA and suggest that GNA represents a promising candidate for canine OS therapy**.**

Funding statement: This research was supported by the National Natural Science Foundation of China (No. 32273078), Natural Science Foundation of Heilongjiang Province (No. ZL2024C020), and Heilongjiang Postdoctoral General Fund (Second Class, No. LBH-Z24094).

Ethical approval: This study strictly followed the international animal welfare and ethical standards, and has passed the animal ethics audit of Northeast Agricultural University (ethical code: NEAUEC20230379, January 01, 2024).

Acknowledgment: We would like to thank FACC for the donation of osteosarcoma cell lines.

Authors contribution: MW and HK conceived and designed the study. GZ, JS, SL and MW executed the experiment and analyzed the cell samples. WW, QH and PL analyzed and interpreted the data. GZ, JS, XL and BY collected research background data. MW, HK and GZ prepared the manuscripts. HF and YZ critically revised the manuscript for important intellectual contents and approved the final version.

Conflict of interest: No potential conflict of interest was reported by the authors.

Data availability: All data generated or analyzed during this study are included in this published article. Further inquiries can be directed to the corresponding author upon reasonable request.

Generative AI statement: The authors declare that no Gen AI/DeepSeek was used in the writing/creation of this manuscript.

REFERENCES

Al-Ostoot FH, Salah S, Khamees HA, *et al.*, 2021. Tumor angiogenesis: Current challenges and therapeutic opportunities. Cancer Treatment and Research Communications 28:100422. doi: 10.1016/j.ctarc.2021.100422.

Aranguren XL, Agirre X, Beerens M, *et al.*, 2013. Unraveling a novel transcription factor code determining the human arterial-specific endothelial cell signature. Blood 122(24):3982-92. doi: 10.1182/blood-2013-02-483255.

Baker M, Robinson SD, Lechertier T, *et al.*, 2011. Use of the mouse aortic ring assay to study angiogenesis. Nature Protocols 7(1):89-104. doi: 10.1038/nprot.2011.435.

Cai WX, Liang L, Ji P, *et al.*, 2011. Experimental study on culture method of human umbilical vein endothelial cells. Chinese Journal of Reparative and Reconstructive Surgery 25(2):139-43.

Chen F, Li YC, Qin N, *et al.*, 2020. RNA-seq analysis identified hormone-related genes associated with prognosis of triple negative breast cancer. Journal of Biomedical Research 34(2):129-38. doi: 10.7555/JBR.34.20190111.

Chen JP, Wang DL, Yang LL, *et al.*, 2014. Ultra-high-performance liquid chromatography tandem mass spectrometry method for the determination of gambogenic acid in dog plasma and its application to a pharmacokinetic study. Biomedical Chromatography 28(12):1854-59. doi: 10.1002/bmc.3231.

Chen Z, Cai H and Ni X, 2024. P02.25.A Tumor microenvironment (TME) Vis-À-Vis anti-vascular treatment in glioblastoma. Neuro-Oncology 26(Supplement 5):v40-v41. doi: 10.1093/neuonc/noae144.128.

Cheng H, Wang YL, Su JJ, *et al.*, 2018. Mechanism of gambogenic acid in resisting angiogenesis of lung cancer *in vitro*. China Journal of Chinese Materia Medica 43(21):4311-16. doi:10.19540/j.cnki.cjcmm.20180601.001.

Du M, Geng T, Yu R, *et al.*, 2023. Smart anti-vascular nanoagent induces positive feedback loop for self-augmented tumor accumulation. Journal of Controlled Release 356(8):595-609. doi:10.1016/j.jconrel.2023.03.021.

Fagiani E, Lorentz P, Kopfstein L, *et al.*, 2011. Angiopoietin-1 and -2 exert antagonistic functions in tumor angiogenesis, yet both induce lymphangiogenesis. Cancer Research 71(17):5717-27. doi: 10.1158/0008-5472.CAN-10-4635.

Gao T, Wang Z and Liu Y, 2023. Matrix metalloproteinase 2 expression and disease-free survival of patients with osteosarcoma: A meta-analysis. Investigación Clínica 64(2):255-62.

Gola C, Iussich S, Noury S, *et al.*, 2020. Clinical significance and in vitro cellular regulation of hypoxia mimicry on HIF-1α and downstream genes in canine appendicular osteosarcoma. The Veterinary Journal 264:105538. doi: 10.1016/j.tvjl.2020.105538.

Gola C, Massimini M, Morello E, *et al.*, 2024. Prognostic significance of Microvessel density and hypoxic markers in canine osteosarcoma: Insights into angiogenesis and tumor aggressiveness. Animals (Basel) 14(22):3181. doi: 10.3390/ani14223181.

Hatami E, Jaggi M, Chauhan SC, *et al.*, 2020. Gambogic acid: A shining natural compound to nanomedicine for cancer therapeutics. Biochimica et Biophysica Acta (BBA): Reviews on Cancer 1874(1):188381. doi: 10.1016/j.bbcan.2020.188381.

Jiang W, Brennen WN, Denmeade SR, *et al.*, 2022. Abstract 6055: Cell confluence growth tracking as a supplement assay for clonogenic assay in prostate cancer radiotherapy combination evaluation. Cancer Research 82(12_Supplement):6055. doi:10.1158/1538-7445.AM2022-6055.

Lee E and Loukopoulos P, 2024. Genetic changes clinically relevant in canine osteosarcoma. Journal of the Hellenic Veterinary Medical Society 75(3):7649-54. doi.org/10.12681/jhvms.32336.

Li S, Zhao Y, Hou X, *et al.*, 2025. Gambogenic acid enhances oxidative stress and apoptosis by suppressing canine osteosarcoma cell growth via autophagy overactivation. Pakistan Veterinary Journal 45(3):1029-44.

Liu X, Zhao M, Mi J, *et al.*, 2014. Simultaneous quantification of MTC-220 and its metabolites in beagle dog plasma by liquid chromatography-tandem mass spectrometry. Journal of Pharmaceutical and Biomedical Analysis 99:1-7.

Liu Y, Huang N, Liao S, *et al.*, 2021. Current research progress in targeted anti-angiogenesis therapy for osteosarcoma. Cell Proliferation 54(9):e13102. doi: 10.1111/cpr.13102.

Massimini M, De Maria R, Malatesta D, *et al.*, 2019. Establishment of three-dimensional canine osteosarcoma cell lines showing vasculogenic mimicry and evaluation of biological properties after treatment with 17-AAG. Veterinary and Comparative Oncology 17(3):376-84. doi: 10.1111/vco.12482.

Mi L, Xing Z, Zhang Y *et al.*, 2024. Unveiling gambogenic acid as a promising antitumor compound: A review. Planta Medica 90(5):353-67. doi: 10.1055/a-2258-6663.

Novikova IA, Kit OI, Ulianova EP, *et al.*, 2016. Analysis of ALK-status of tumor tissue in patients with non-small cell lung cancer (NSCLC) using immunohistochemistry (IHC). Journal of Clinical Oncology 34(15 Supplement):e20071.

Pan Z, Xu T, Bao L, *et al.*, 2022. CREB3L1 promotes tumor growth and metastasis of anaplastic thyroid carcinoma by remodeling the tumor microenvironment. Molecular Cancer 21(1):190. doi: 10.1186/s12943-022-01658-x.

Pant K, Richard S, Peixoto E, *et al.*, 2025. Cholangiocyte ciliary defects induce sustained epidermal growth factor receptor signaling. Hepatology 81(4):1132-1145. doi: 10.1097/HEP.0000000000001055.

Park W, Wollmann G, Urbiola C, *et al.*, 2017. CBIO-32. Sprouty-2 enhances tumor-propagating potential of glioma cells. Neuro-Oncology 19(Supplement 6):vi39. doi: 10.1093/neuonc/nox168.150.

Prisco AR, Bukowy JD, Hoffmann BR, *et al.*, 2014. Automated quantification reveals hyperglycemia inhibits endothelial angiogenic function. PLoS One 9(4):e94599. doi: 10.1371/journal.pone.0094599.

Rizzo VL, Levine CB and Wakshlag JJ., 2017. The effects of sulforaphane on canine osteosarcoma proliferation and invasion. Veterinary and Comparative Oncology 15(3):718-30. doi: 10.1111/vco.12212.

Romanucci M, De Maria R, Morello EM, *et al.*, 2023. Editorial: Canine osteosarcoma as a model in comparative oncology: Advances and perspective. Frontiers in Veterinary Science 10:1141666. doi: 10.3389/fvets.2023.1141666.

Stein PA, Toret CP, Salic AN, *et al.*, 2002. A novel centrosome-associated protein with affinity for microtubules. Journal of Cell Science 115(Pt 17):3389-3402. doi: 10.1242/jcs.115.17.3389.

Sun R, Zhang HM and Chen BA, 2018. Anticancer activity and underlying mechanism of neogambogic acid. Chinese Journal of Natural Medicines 16(9):641-43. doi: 10.1016/S1875-5364(18)30103-1.

Szewczyk M, Lechowski R and Zabielska K, 2015. What do we know about canine osteosarcoma treatment? Review. Veterinary Research Communications 39(1):61-67. doi: 10.1007/s11259-014-9623-0.

Tavakolikazerooni H, Tariq M, Yu H, *et al.*, 2025. Melatonin modulates necroptosis and enhances antioxidant defense during PGF-induced luteal regression in heat-exposed rats. Pakistan Veterinary Journal 45(1):205-215.

Tu HQ, Qin XH, Liu ZB, *et al.*, 2018. Microtubule asters anchored by FSD1 control axoneme assembly and ciliogenesis. Nature Communications 9(1):5277. doi: 10.1038/s41467-018-07664-2.

Wu J, Wang D, Zhou J, *et al.*, 2022. Gambogenic acid induces apoptosis and autophagy through ROS-mediated endoplasmic reticulum stress via JNK pathway in prostate cancer cells. Phytotherapy Research 37(1):310-28. doi: 10.1002/ptr.7614.

Wu Y, Chen S, Shao Y, *et al.*, 2023. KLF5 promotes tumor progression and Parp inhibitor resistance in ovarian cancer. Advanced Science 10(31):e2304638. doi: 10.1002/advs.202304638.

Xiao D, Ran H, Chen L, *et al.*, 2025. FSD1 inhibits glioblastoma diffuse infiltration through restriction of HDAC6-mediated microtubule deacetylation. Science China Life Sciences 68(3):673-688. doi: 10.1007/s11427-024-2616-7.

Xiong Y, Scerbo MJ, Seelig A, *et al.*, 2020. Islet vascularization is regulated by primary endothelial cilia via VEGF-A-dependent signaling. Elife 9:e56914. doi: 10.7554/eLife.56914.

Xu J and Tang Z, 2024. Progress on angiogenic and antiangiogenic agents in the tumor microenvironment. Frontiers in Oncology 14:1491099. doi: 10.3389/fonc.2024.1491099.

Xun J, Jiang X, Liu B, *et al.*, 2024. Neogambogic acid enhances anti-PD-1 immunotherapy efficacy by attenuating suppressive function of MDSCs in pancreatic cancer. International Immunopharmacology 139:112696. doi: 10.1016/j.intimp.2024.112696.

Yang S, Zhou X, Li R, *et al.*, 2017. Optimized PEI-based transfection method for transient transfection and lentiviral production. Current Protocols in Chemical Biology 9(3):147-57. doi: 10.1002/cpch.25.

You M, Fu J, Lv X, *et al.*, 2023. Saikosaponin b2 inhibits tumor angiogenesis in liver cancer via down-regulation of VEGF/ERK/HIF-1α signaling. Oncology Reports 50(1):136. doi: 10.3892/or.2023.8573

Zhao Y, Wang C, Yang T, *et al.*, 2022. Chlorogenic acid alleviates chronic stress-induced duodenal ferroptosis via the inhibition of the IL-6/JAK2/STAT3 signaling pathway in rats. Journal of Agricultural and Food Chemistry 70(14):4353-61. doi: 10.1021/acs.jafc.2c01196.